Aalborg Universitet

A Simple Operation Approach for Modular Multilevel Converter Under Grid Voltage Swell in Medium-Voltage Microgrids

Xiao, Qian; Jin, Yu; Chen, Linglin; Yu, Xiaodan; Liu, Huiqiao; Teodorescu, Remus; Blaabjerg, Frede

A Simple Operation Approach for Modular Multilevel Converter Under Grid Voltage Swell in Medium-Voltage Microgrids

QIAN XIAO[1], **YU JIN**[2,5], **LINGLIN CHEN**[3], **XIAODAN YU**[1],
HONGJIE JIA[1], (Senior Member, IEEE), **HUIQIAO LIU**[4],
REMUS TEODORESCU[5], (Fellow, IEEE), AND
FREDE BLAABJERG[5], (Fellow, IEEE)

[1]Key Laboratory of Smart Grid of Ministry of Education, Tianjin University, Tianjin 300072, China
[2]Department of Electrical Engineering and Automation, Harbin Institute of Technology, Harbin 150006, China
[3]Department of Electrical and Electronics Engineering, University of Nottingham, Nottingham NG7 2RD, U.K.
[4]Department of Automation Engineering, Zhonghuan Information College, Tianjin University of Technology, Tianjin 300380, China
[5]Department of Energy Technology, Aalborg University, 9220 Aalborg, Denmark

Corresponding authors: Yu Jin (hitjy19940213@163.com) and Xiaodan Yu (yuxd@tju.edu.cn)

ABSTRACT Modular multilevel converter (MMC) is drawing more and more attention in medium-voltage microgrid applications. Large-scale switching-off loads and grid faults may lead to the voltage swell in microgrid, where MMC should have the ride-through ability. In this paper, a simple operation approach with the fundamental and irregular zero-sequence voltage (ZSV) injection is proposed for MMC under grid voltage swell condition. First, the fundamental ZSV injection is applied to adjust the modulation margin of three phases where the amplitude values of modulation waves in each phase can be the same. Then, if the amplitudes with fundamental ZSV injection are still in over-modulation status, the new irregular ZSV injection is added to further enlarge the operation region. In addition, the limitation of the irregular ZSV injection is analyzed. Simulation and experimental results of MMC under different grid voltage swell conditions verify the effectiveness of the proposed operation approach.

INDEX TERMS Modular multilevel converter (MMC), microgrid, grid fault, grid voltage swell, fault-tolerant operation, zero-sequence voltage injection.

I. INTRODUCTION

The rapid penetration of renewable energy, such as wind power and solar energy, dramatically draw more attention and changes in modern distributed power system and microgrid [1]–[3]. With the growth of the capacity of this renewable energy system to be integrated into the microgrids, medium, and high voltage power converter are widely applied in the power conversion application [4], [5]. However, with the increasing demand and generation in the microgrids, the harsher requirements have been proposed for the power converters, such as more flexible power conversion, simpler structure and high operation reliability [6], [7]. As one of the most promising medium and high voltage converters,

MMC has been widely applied in various applications such as voltage source converter (VSC) based high voltage direct current (HVDC) [8], STATCOM [9], motor drive [10], DC ship microgrid [11], energy storage system [12] and power electronic transformers [13]. Due to its modularity, scalability, excellent harmonic performance, relatively low switching frequency, fault ride-through ability, MMC has already been applied in AC microgrid application [14].

For the microgrid application where MMC is connected to distributed synchronous generators and grid loads, the large-scale loads switching off may lead to the grid voltage swell [15]. In the practical application, most grid-connected standards require the converter to possess the low voltage ride through (LVRT) capabilities [16]–[18]. Also, high voltage ride through (HVRT) capabilities are expected to be a mandatory requirement for wind farms considering the rapid

The associate editor coordinating the review of this manuscript and approving it for publication was Jun Wu.

growth of wind power capacity and improvement of the grid connection standards [15]. The HVRT guideline for grid-connected converters are initially formulated by the Australia government [19]. This standard requires the grid connected converter to keep connected for a short period even under grid voltage swell occasions.

Many researches have been carried out to realize the HVRT capability. Conventionally, the dynamic voltage restorer (DVR) and static synchronous compensators (STATCOM) are applied [20], [21]. DVR devices are series-connected to the grid and can generate voltage to maintain the grid voltage stable, and STATCOM will adjust the grid voltage based on the injection of negative-sequence current. However, the additional devices inevitably increase the cost of the system.

In [22], a chopper circuit is applied to suppress the reverse power flow under grid voltage swell. In [23], a series-connected resistance is applied in the converter to provide reactive power support. However, this method increases the complexity of the system and lower the system efficiency. In addition, a vector hysteresis controller is adopted during the grid voltage swell, which provides a good dynamic response of the current controller and provides the HVRT ability for grid-connected converter [24]. Another fault ride-through operation scheme for two-level converter under grid voltage swell is presented with a modified space vector modulation (SVM) [25]. This method can significantly improve the ride-through ability for severe voltage swell. However, the SVM method is much more complicated for MMC, and the converter may work in the over-modulation condition, which may lead to current distortions. In addition, few papers focus on the operation approach under grid voltage swell of MMC. For a submodule fault ride-through of MMC, zero-sequence voltage (ZSV) has been injected to realize the normal operation with a lower output voltage in the faulty phase [26]. When the grid voltage swell occurs in MMC, the over-modulation will occurs in the faulty phase, and this will lead to the current distortion, and even the collapse of the control system which may destroy the devices.

In this paper, a simple operation approach with a fundamental and an irregular ZSV injection is proposed for MMC under grid voltage swell. The rest of the paper is outlined as follows. Section II gives the basic topology, the mathematic model, and the overall operation strategy of MMC. Section III analyzes the proposed operation approach under grid voltage swell in detail. A three-phase simulation model is established and verified in Section IV, proving the effectiveness of the proposed method. In Section V, the experimental results on a three-phase laboratory prototype validate the effectiveness of the proposed ride-through approach under grid voltage swell.

II. TOPOLOGY AND WORKING PRINCIPLE OF MMC

In this section, the topology and equivalent circuit of MMC are presented first. Then, based on the equivalent circuit, the overall control scheme of MMC is described.
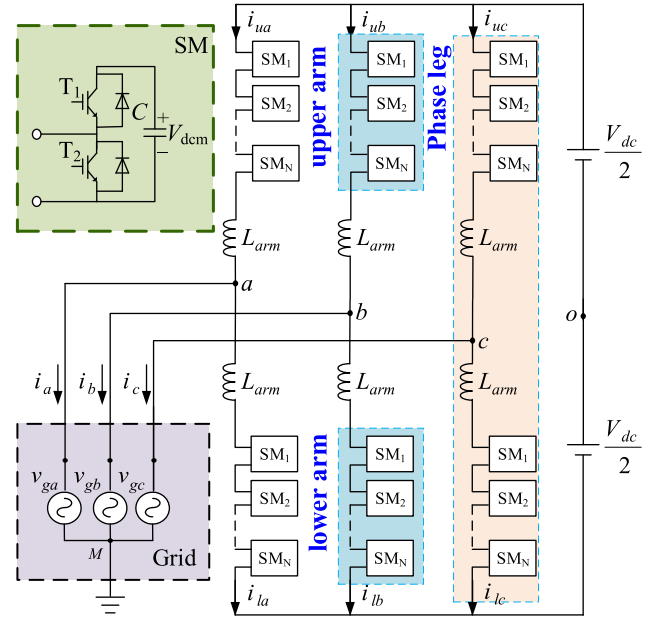

FIGURE 1. Circuit topology of MMC.

A. TOPOLOGY OF MMC

As is shown in Fig. 1, MMC is composed of three phase legs, each of which contains the upper and the lower arm. There are N submodules (SMs) in each arm, and each SM consists of two power switches with parallel-connected diodes and one capacitor. The upper and the lower arm include one arm inductor, L_{arm}, and are connected to a common terminal which is connected to the grid. v_{gj} are the three-phase grid voltages, and i_j are the three-phase output currents (j = a, b, c). i_{uj} and i_{lj} are the currents of the upper and the lower arm. V_{dc} is the DC side voltage of MMC, and V_{dcm} is the rated capacitor voltage of each SM.

B. EQUIVALENT CIRCUITS OF MMC

According to the MMC topology in Fig. 1, the equivalent circuits of MMC can be expressed as shown in Fig. 2 (a). It includes the AC path and the DC path, the equivalent circuits of which are given respectively as Fig. 2 (b) and Fig. 2 (c). The AC path controls the output currents of the converter, and the DC path controls the internal circulating currents of MMC.

The AC path can be characterized as

$$\begin{cases} u_{diffj} = \dfrac{u_{lj} - u_{uj}}{2} \\ i_j = \dfrac{i_{uj} - i_{lj}}{2} \\ R_{eq}i_j + L_{eq}\dfrac{di_j}{dt} = u_{diffj} - U_{sj} \end{cases} \quad (1)$$

where R_{eq} and L_{eq} are expressed as

$$\begin{cases} R_{eq} = R_{arm}/2 \\ L_{eq} = L_{arm}/2 \end{cases} \quad (2)$$
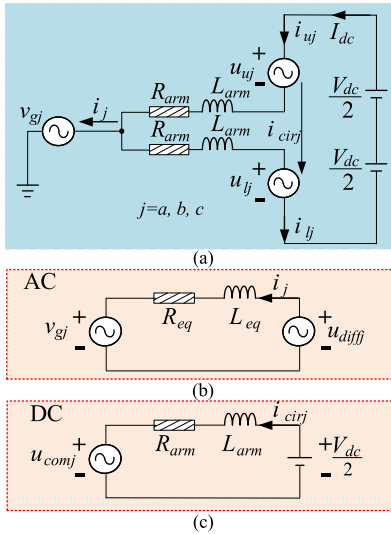
FIGURE 2. Equivalent circuits of MMC. (a). Overall equivalent circuit. (b). Equivalent circuit of the AC path. (c). Equivalent circuit of the DC path.

where R_{arm} and L_{arm} are arm resistor and arm inductor, R_{ac} and L_{ac} are AC output resistor and arm inductor.

Then, the DC path can be characterized as

$$\begin{cases} u_{comj} = \dfrac{u_{lj} + u_{uj}}{2} \\ R_{arm}i_{cirj} + L_{arm}\dfrac{di_{cirj}}{dt} = \dfrac{U_{dc}}{2} - u_{comj} \end{cases} \quad (3)$$

Therefore, the MMC can be effectively controlled with the AC path and the DC path.

C. OVERALL CONTROL MODEL
The overall control scheme of MMC is shown in Fig. 3, which can be divided into four parts, output current control, arm energy and circulating current control, individual voltage control and grid fault ride-through approach.

The output current control is designed to control the output currents of MMC. In this paper, a decoupled PI controller in *dq* frame is adopted to control the output currents, which is expressed as

$$\begin{bmatrix} V_d \\ V_q \end{bmatrix} = \begin{bmatrix} R_{eq} + j\omega L_{eq} & -\omega L_{eq} \\ -\omega L_{eq} & R_{eq} + j\omega L_{eq} \end{bmatrix} \begin{bmatrix} I_d \\ I_q \end{bmatrix} \quad (4)$$

The grid voltage is added as a feed-forward component. In addition, in grid voltage swell condition, an additional zero-sequence voltage (ZSV) is injected to maintain the normal operation of MMC.

The arm energy and circulating current control is used to control and balance the capacitor voltage between each arm. The arm energy control includes sum energy control and delta energy control, which are designed to control the sum and the difference between the capacitor voltages of the upper and the lower arm. The corresponding circulating current reference calculated by arm energy control will be sent to the circulating current control.

For the sum energy control, the circulating current reference is a DC component and can be expressed as

$$i^*_{cirj1} = (K_{psum} + K_{isum}/s)(2V_{dc} - \text{LPF}\{V_{\Sigma j}\}) \quad (5)$$

where LPF is the low pass filter; K_{psum} and K_{isum} are the coefficients of the PI controller; $V_{\Sigma j}$ is expressed as

$$V_{\Sigma j} = \sum V^{up}_{dcjn} + \sum V^{low}_{dcjn} \quad (6)$$

where V^{up}_{dcjn} and V^{low}_{dcjn} are the capacitor voltages of each SM ($n = 1, 2, \ldots, N$).

For the delta energy control, the circulating current reference is a fundamental AC component and can be expressed as

$$i^*_{cirj2} = K_{pdelta}(0 - \text{LPF}\{V_{\Delta j}\})\sin \omega t \quad (7)$$

where K_{pdelta} is the coefficient of the P controller; $V_{\Delta j}$ is expressed as

$$V_{\Delta j} = \sum V^{up}_{dcjn} - \sum V^{low}_{dcjn} \quad (8)$$

The final circulating current reference can be derived as

$$i^*_{cirj} = i^*_{cirj1} + i^*_{cirj2} \quad (9)$$

For the circulating current control, the proportional-integral-resonant (PIR) controllers are used in this paper. For the DC circulating current component, the PI controller can effectively track the DC component. In addition, the two resonant controllers are designed individually to realize accurate control of the fundamental circulating current and suppress the second-order circulating currents. The control parameters design principle of the PIR controller can also be found in [27].

In this paper, phase-shift PWM is applied and the individual voltage control is designed to realize the capacitor voltage balancing between SMs within each arm. The basic principle and control parameter are not discussed in this paper and they can be found in [28].

For fault ride-through operation, it will calculate the injected ZSV reference based on the swell depth of the grid voltage. The detailed operation approach will be discussed in the next section.

III. OPERATION APPROACH UNDER VOLTAGE SWELL
In this section, the problem of grid voltage swell is introduced first. Then, the proposed operation approach under grid voltage swell is illustrated in detail.

It should be noted that this paper focuses on the operation approach after the detection of the grid voltage swell. The detection method can be found in [29], and this paper will not discuss the detection method in detail.

A. PROBLEM OF GRID VOLTAGE SWELL
The phasor diagram of MMC under normal operation is depicted in Fig. 4, where v_{gj} is the grid voltage, and v_j is the output phase voltages ($j = a, b, c$). v_{ab}, v_{bc}, v_{ca}, are the line-to-line voltages of MMC.
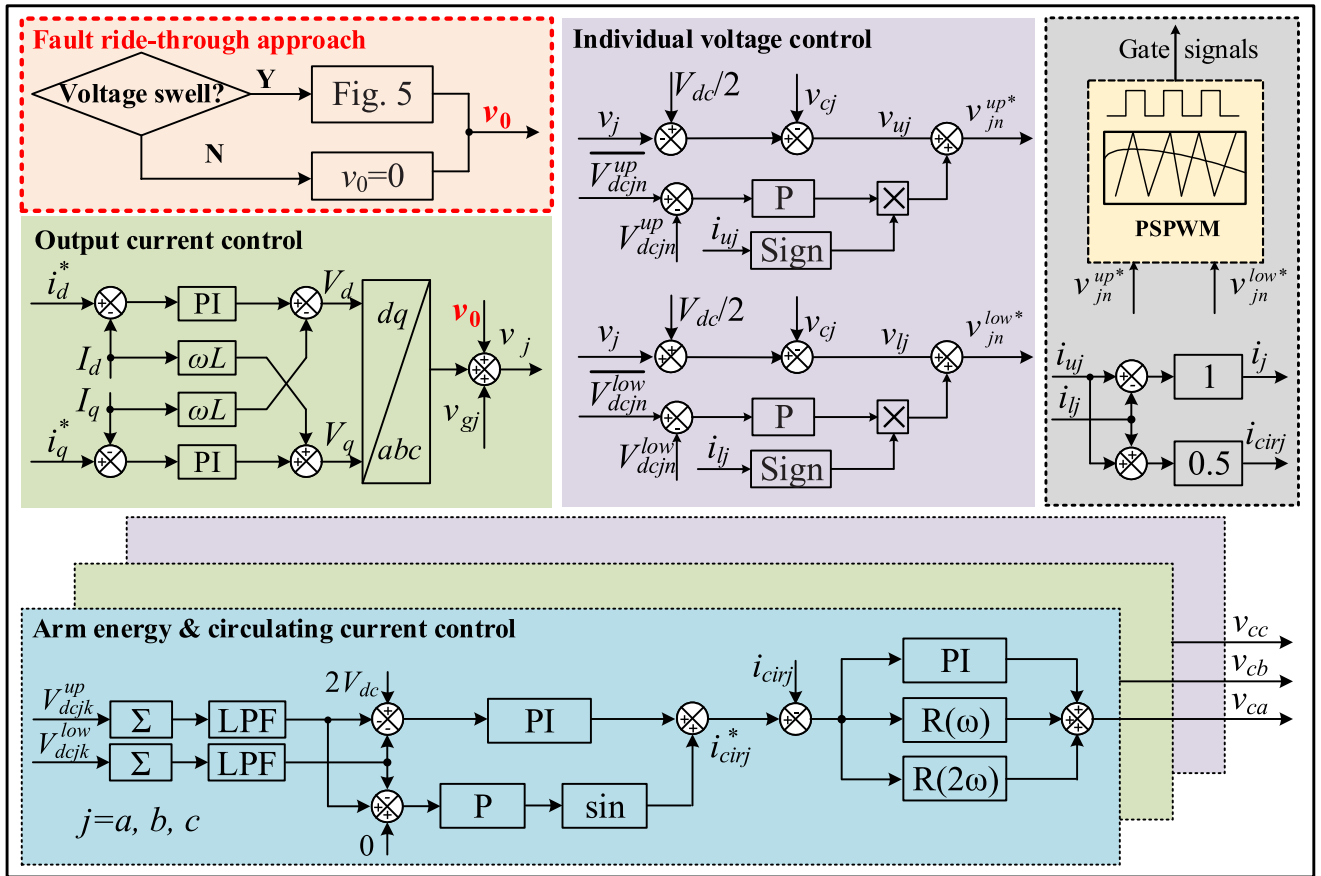
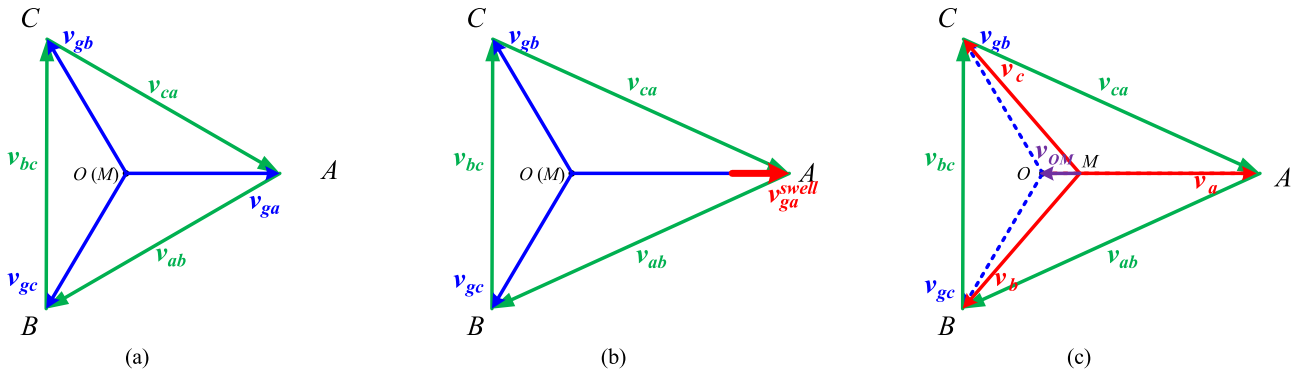**FIGURE 3.** The overall control scheme of MMC.

FIGURE 4. Phasor diagram of different operation status. (a). Phasor diagram under normal operation. (b). Phasor diagram under grid voltage swell. (c). Phasor diagram under normal operation with fundamental ZSV injection.

As shown in Fig.4 (a), the DC voltage is able to sustain the grid voltage during normal operation. However, when grid swell occurs in phase A, the output voltage of phase A may be unable to sustain the grid voltage.

Before the discussion of grid voltage swell, the depth of the grid voltage swell is defined as D.

$$V_{ga}^{swell} = (1 + D)V_g \qquad (10)$$

where V_{ga}^{swell} is the amplitude of the grid swell voltage, V_g is the amplitude of the grid voltage.

Supposing the grid voltage swell occurs in phase A, where D is 0.2, the phasor diagram can be given as shown in Fig. 4 (b). As a result, the over-modulation phenomenon will arise, which may lead to current distortion, unbalanced capacitor voltage, and even collapse of the control system. As a result, the operation approach under grid voltage swell is necessary for the stable operation of MMC.

It should be mentioned that the fundamental ZSV (FZSV) injection can adjust the modulation margin between the faulty phase and the healthy phases, as shown in Fig. 4 (c).
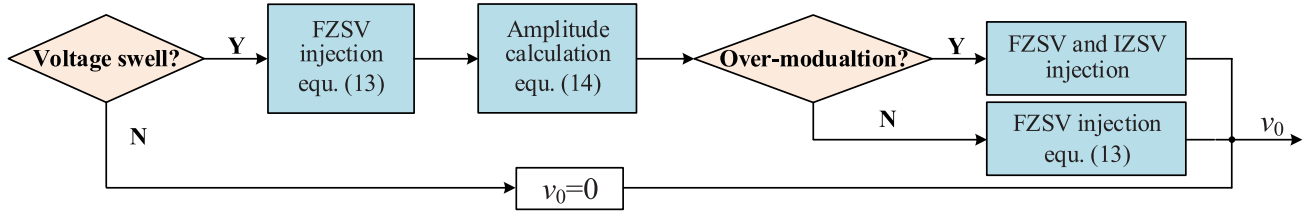
FIGURE 5. Fault ride-through operation approach under grid voltage swell.

FIGURE 6. The injection principle of IZSV. (a). The modulation waves with FZSV and IZSV. (b). The injected IZSV.

In Fig. 4 (c), v_{OM} represents the injected FZSV. This paper mainly focus on the component of the injected ZSV to withstand a higher voltage swell. In other words, this paper try to generate a higher line-to-line voltage under the same grid voltage swell.

The overall fault ride-through operation approach under grid voltage swell is shown in Fig. 5. First of all this paper injects a FZSV component to adjust the amplitude of the modulation waves of each phase. Then based on the injected FZSV, the irregular ZSV component is injected in the over-modulation occasion to realize a higher tolerance for the grid voltage swell. These two parts will be discussed in details in the following subsections.

B. FZSV INJECTION AND ANALYSIS

The FZSV injection mainly focus on balancing the amplitude of the modulation waves between the three phases, which will provide a higher operation tolerance for grid voltage swell.

During normal operation, the amplitude of the modulation waves are supposed to be the same with that of the grid voltages, due to the fact that the voltage across the arm inductor can be neglected. With this assumption, the FSZV can be derived as follows.

Supposing the grid depth of the voltage swell in phase A is D, the injected FZSV is expressed as

$$v_0^F = m \cdot v_{ga} \qquad (11)$$

With the FZSV, the modified amplitudes of voltage references in phase A, phase B and phase C, V_a, V_b and V_c, satisfy the relation:

$$V_a + V_0^F = (1+D)V_g$$
$$V_b^2 = V_c^2 = (V_{OH} + V_0^F)^2 + (V_{CH})^2$$
$$V_{OH} = {}^1/_2 V_g, V_{CH} = \sqrt{3}/_2 V_g \qquad (12)$$

where V_b and V_c are derived based on cosine theorems of triangles.

As a result, the amplitude of voltage references can be expressed as

$$V_a = (1+D-m)V_g \qquad (a)$$
$$V_b = V_c = V_g\sqrt{1+m^2+m} \qquad (b) \qquad (13)$$

In order to balance the amplitude of the modulation waves, make (13) (a) equal to (13) (b)
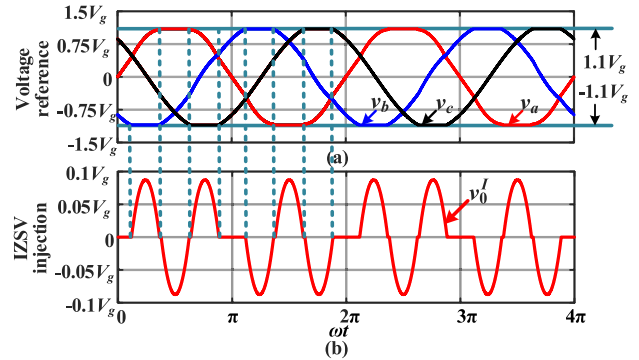
$$(1+D-m) = \sqrt{1+m^2+m} \qquad (14)$$

The index of the injected FZSV can be further derived as

$$m = \frac{D^2 + 2D}{3 + 2D} \qquad (15)$$

Then, the amplitude of the modulation wave can be expressed as

$$V_a = V_b = V_c = \frac{D^2 + 3D + 3}{3 + 2D}V_g \qquad (16)$$

C. IRREGULAR ZSV INJECTION WITH HIGHER OPERATION RANGE

With the calculated amplitude of (16), even with the FZSV, there is still a risk of over-modulation. In order to avoid the over-modulation occasion, the irregular ZSV (IZSV) injection is further applied to improve the operation range for grid voltage swell. The principle of the IZSV injection is shown in Fig. 6, where the maximum output voltage is assumed to be 1.1 V_g. Fig. 6 (a) gives the final output voltage references with the FZSV and IZSV injection and Fig. 6 (b) shows the injected IZSV.

With the FZSV injection discussed in the last subsection, if the over-modulation occurs in one phase, the modulation wave of this phase will be clamped to the limit, then the other two phases inject the same IZSV to generate the desired line-to-line voltage. The IZSV injection can further improve the operation tolerance for the grid voltage swell.

However, there is a boundary for the IZSV injection, especially when the modulation waves are asymmetric. The IZSV injection boundary is discussed as follows. The derivation is based on the FZSV injection in Fig. 4 (c).
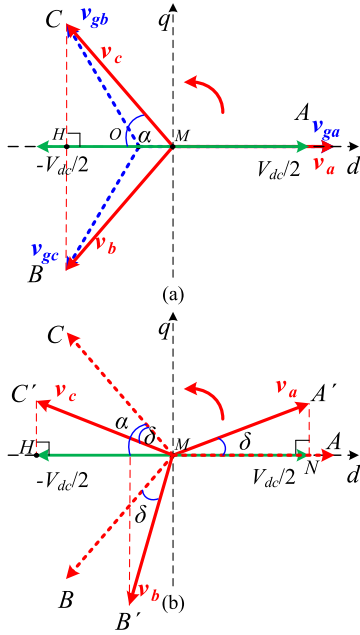
FIGURE 7. The vector and projection of modulation waves. (a). The vector and projection of modulation waves during normal operation. (b). The vector and projection of modulation waves under the grid voltage swell.

As is shown in Fig. 7 (a), during normal operation with the FZSV injection, the vector of v_{ga}, v_{gb}, and v_{gc} are projected to the d axis, and the projections represent the real-time value of the modulation wave. The three vectors rotate together with the phase angle of the grid.

Based on the projection analysis and schematic in Fig. 6 (b), the occasion with the limit of the IZSV injection is depicted as shown in Fig. 7 (b), where the relationship between the three vectors can be expressed as (17) due to the injection of FZSV.

$$|v_a| = |v_b| = |v_c| \qquad (17)$$

In Fig. 7 (b), vector MA, MB and MC rotate to MA', MB' and MC' at the angle of δ. According to the HL law of triangle congruence, the two triangles are congruent.

$$\begin{aligned} MA' &= MB' \\ MH &= MN \end{aligned} \Rightarrow \Delta MA'N \cong \Delta MC'H \qquad (18)$$

As a result, the angle α and δ satisfy the constraint

$$\alpha - \delta = \delta \qquad (19)$$

The maximum amplitude of the modulation wave with FZSV injection should be

$$V_{a\,\max} = V_{b\,\max} = V_{c\,\max} = 0.5 V_{dc}/\cos\delta \qquad (20)$$

Based on cosine theorems of triangles in Fig. 7 (a), α satisfy the relation

$$\cos\alpha = \frac{V_{OH} + V_0^F}{V_c} = \frac{2D^2 + 6D + 3}{2D^2 + 6D + 6} \qquad (21)$$

TABLE 1. Simulation parameters of MMC.

Items	Symbols	Values
Grid line voltage	V_{gl}	5.5 kV
Rated frequency	f	50 Hz
Rated direct voltage	V_{dc}	10 kV
Arm inductance	L_{arm}	6 mH
Carrier frequency	$f_{carrier}$	1 kHz
Total number of SMs per arm	N	10
Capacitor voltage	V_{sm}	1 kV
SM capacitance	C	2 mF

TABLE 2. Simulation scenarios.

Scenarios	Grid voltage swell (D)	Output currents	IZSV
Case 1	0.2	30 A	No
Case 2	0.4		Yes

Based on the triangle principle, it can be

$$\cos\delta = \sqrt{\frac{1 + \cos\alpha}{2}} \qquad (22)$$

Substituting (19) - (22) to (16), the maximum voltage swell MMC can support should meet the following constraint

$$\left(\frac{V_{dc}}{V_g}\right)^2 = D^2 + 3D + 3$$

The maximum grid voltage swell can be expressed as

$$D = \sqrt{\left(\frac{V_{dc}}{V_g}\right)^2 - \frac{3}{4}} - \frac{3}{2} \qquad (23)$$

IV. SIMULATION RESULTS

In order to verify the effectiveness of the proposed operation approach under grid voltage swell, a three-phase MMC model is established in MATLAB/SIMULINK based on the circuit in Fig. 1. All the controllers are shown in Fig. 3. The simulation parameters are given in Table 1, and the simulation scenarios are shown in Table 2. It should be noted the detection method for grid voltage swell in [29] is applied in this paper. Two simulation cases are designed, where the swell of the grid voltage are 0.2 and 0.4 individually. The output currents are set as 30 A.

The simulation results of Case 1 are shown in Fig. 8. As is shown in Fig. 8 (a), the system is in normal operation status before 0.5 s. At the time of 0.5 s, the grid voltage swell occurs with a depth of 0.2. The output currents are shown in Fig. 8 (b), where the amplitude of output currents remain stable at about 30 A before and after the grid voltage swell, indicating the proposed operation approach can effectively control the output current under grid voltage swell. The zoomed-in view of the output currents, during 0.4 s to 0.5 s and 0.6 s to 0.7 s, are also shown in Fig. 8 (b), where there is almost no current distortion after grid voltage swell. Fig. 8 (c) shows the capacitor voltages, where it can be clearly seen that the capacitor is about 1000 V before the grid voltage swell. After 0.5 s, the capacitor voltages still stabilize at

FIGURE 8. Simulation results with grid voltage swell $D = 0.2$ (0.5 s: Grid voltage swell). (a). Grid voltages waveforms. (b). Output currents. (c). Output voltage references. (d). Capacitor voltages. (e). Injected ZSV.

about 1000 V, demonstrating the capacitor voltage control ability of the proposed operation approach. Fig. 8 (d) gives the three-phase output references. It can be seen that before

0.5 s, the amplitudes of the output references are almost the same as the grid voltages. After 0.5 s, the amplitude of the output voltage reference in the faulty phase is much lower
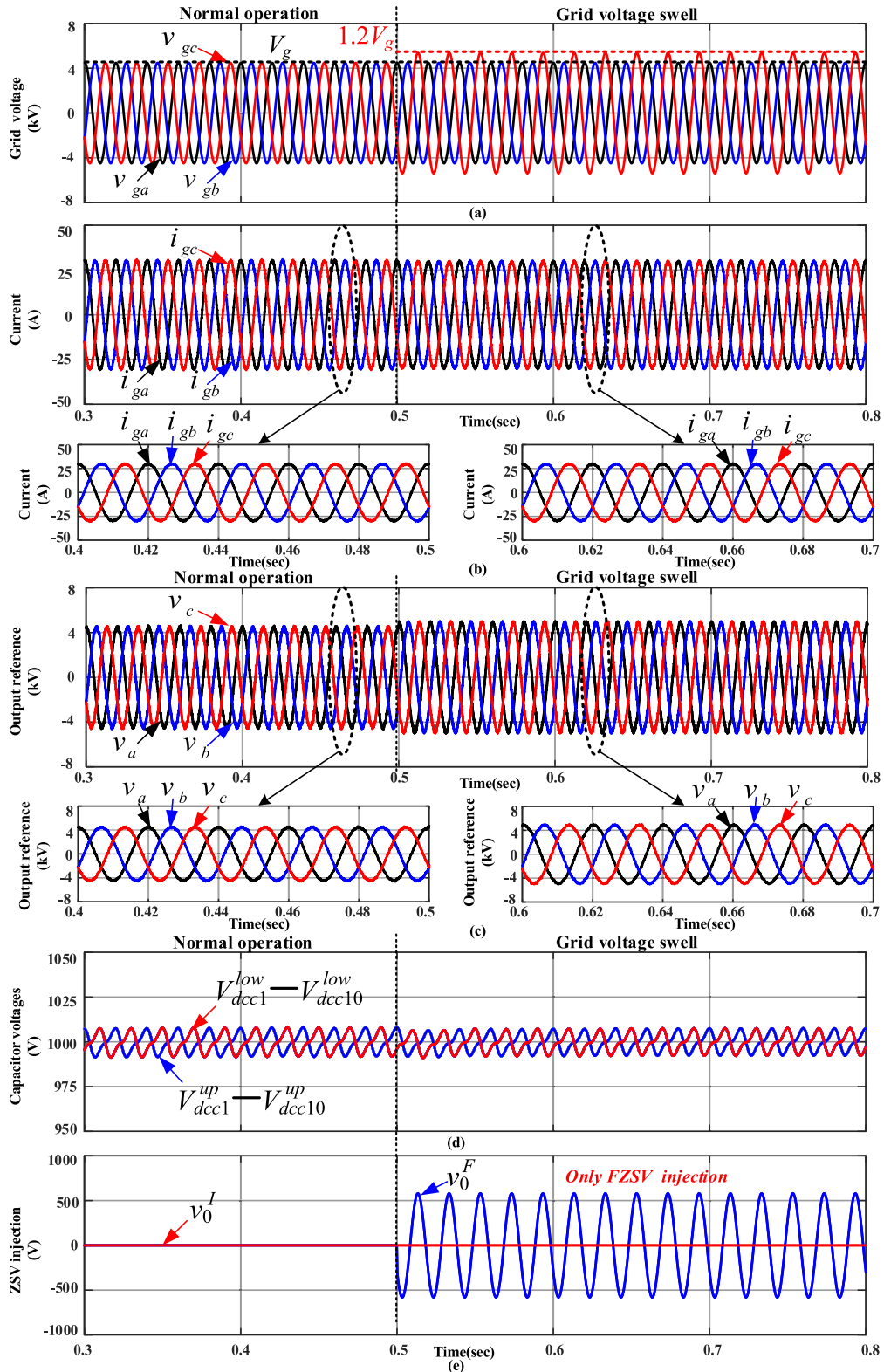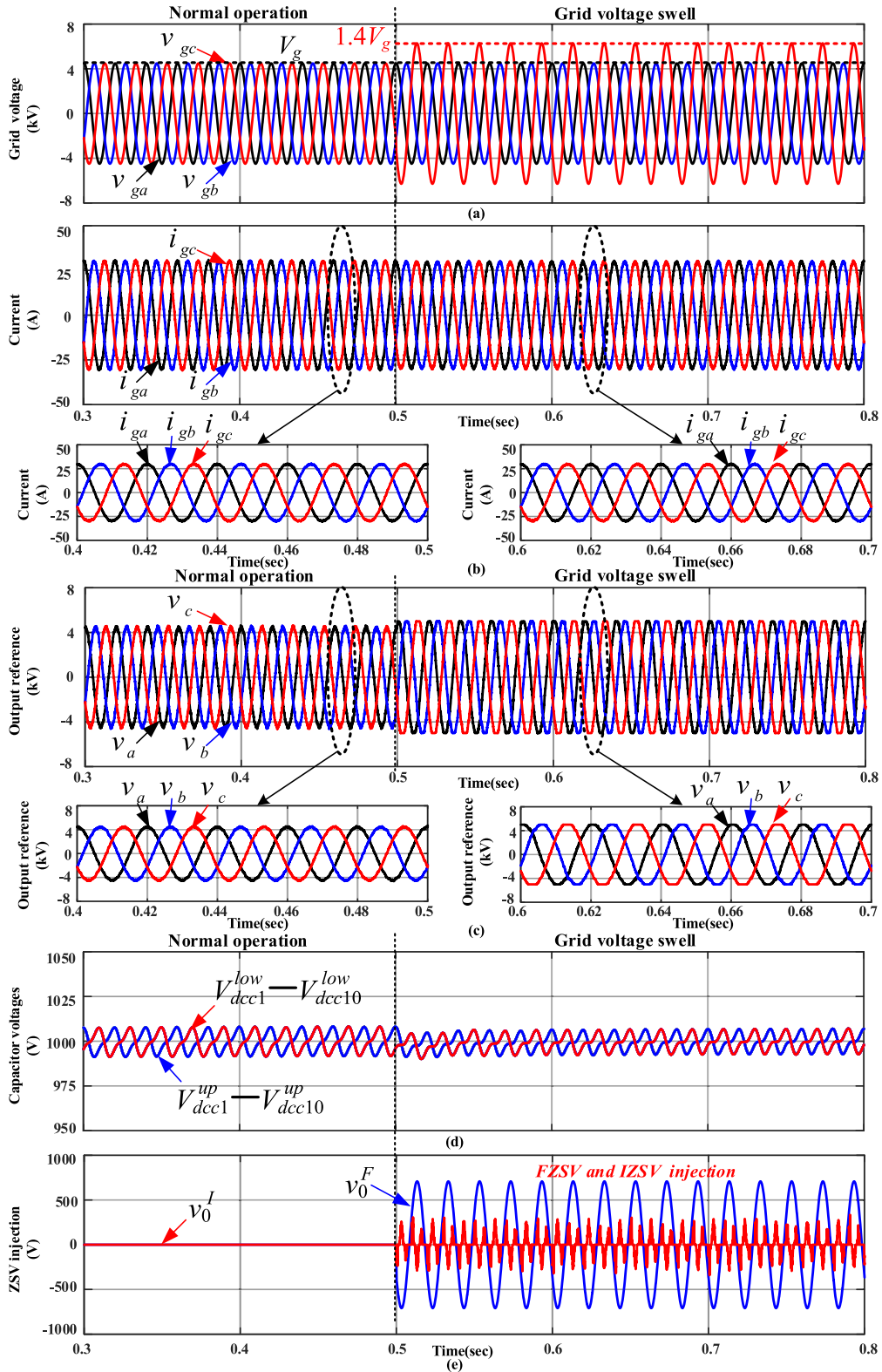
FIGURE 9. Simulation results with grid voltage swell *D* = 0.4 (0.5 s: Grid voltage swell). (a). Grid voltages waveforms. (b). Output currents. (c). Output voltage references. (d). Capacitor voltages. (e). Injected ZSV.

than the amplitude of that of the phase-to-ground voltage, due to the injection of ZSV. The injected FZSV and IZSV are shown in Fig. 8 (e). As is shown in Fig. 8 (e), the injected

ZSV remains at 0 during the normal operation. After 0.5 s, the grid voltage swell with a depth of 0.2 occurs. It can be seen that in this case, the FZSV is injected. However, there is no

TABLE 3. Experiment parameters.

Items	Symbols	Values
Grid voltage	V_g	30 V
Rated frequency	f	50 Hz
Rated direct voltage	U_{dc}	70 V
Arm inductance	L_{arm}	10 mH
Carrier frequency	$f_{carrier}$	1kHz
Total number of SMs per arm	N	4
Capacitor voltage	U_{sm}	17.5 V
SM capacitance	C	2 mF

necessity to inject the IZSV. The effectiveness of the proposed operation approach is thus verified with $D = 0.2$ for a grid voltage swell.

The simulation results of Case 2 are shown in Fig. 9. The grid voltage is shown in Fig. 9 (a), where the system is in normal operation status before 0.5 s. At the time of 0.5 s, the grid voltage swell occurs with a depth of 0.4. Fig. 9 (b) depicts the output currents, where the amplitude of output currents remain stable at about 30 A before and after the grid voltage swell, indicating the proposed operation approach can effectively control the output current under grid voltage swell. The zoomed-in view of the output currents, during 0.4 s to 0.5 s and 0.6 s to 0.7 s, are also exhibited in Fig. 9 (b), where there is almost no current distortion after grid voltage swell. The capacitor voltages are shown in Fig. 9 (c), where the capacitor voltages are about 1000 V before the grid voltage swell. After 0.5 s, the capacitor voltages remain stable at about 1000 V, verifying the capacitor voltage control ability of the proposed operation approach.

Fig. 9 (d) shows the three-phase output references. It can be seen that before 0.5 s, the amplitudes of the output references are almost the same with that of the grid voltages. After 0.5 s, the amplitude of the output voltage reference in the faulty phase is much lower than the amplitude of the phase-to-ground voltage, and is clamped to the maximum output voltage due to the injection of FZSV and IZSV. As is shown in Fig. 9 (e), the injected ZSV remains at 0 during the normal operation. However, after 0.5 s, when the grid voltage swell with a depth of 0.4 occurs, both the FZSV and the IZSV are injected keep the normal operation of the MMC. The simulation results demonstrate the effectiveness of the proposed operation approach with $D = 0.4$ for a grid voltage swell.

V. EXPERIMENTAL RESULTS

A three-phase down-scaled MMC laboratory prototype is implemented to verify the proposed operation approach by experiments. The experiment parameters are listed in Table 3. The prototype works in inverter mode and the output terminals of which are connected to a three-phase programmable AC source. The frequency of the PS-PWM is 1 kHz. As is shown in Fig. 10, dSPACE of 1006 works as the central controller. Each arm contains 4 SMs. The intelligent power module, PSS15S92F6-AG manufactured by MIT-SUBISHI ELECTRONIC, is employed as the switch in SM.
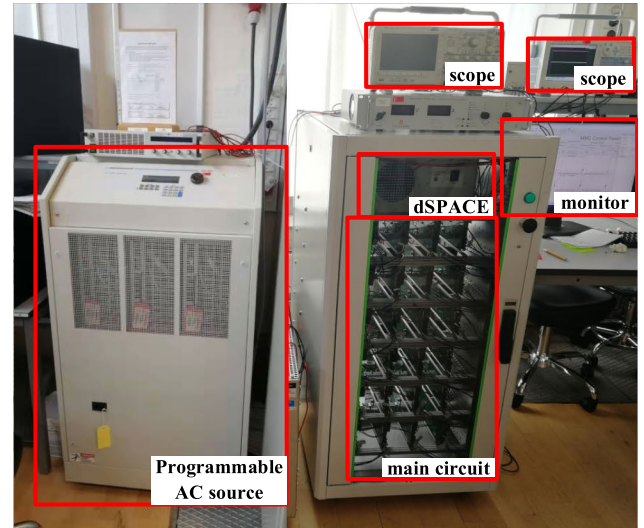
FIGURE 10. The prototype of the three-phase down-scaled MMC.
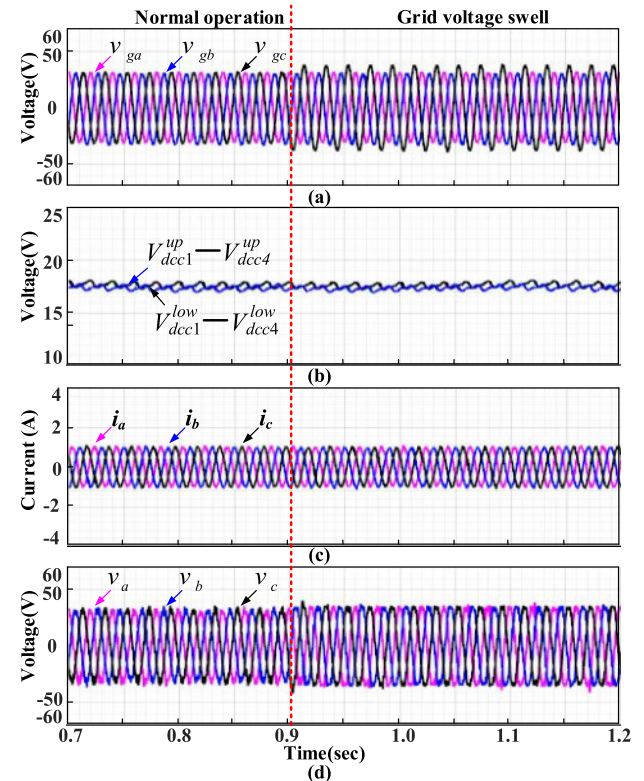
FIGURE 11. Experimental waveforms of proposed operation approach under grid voltage swell with depth of 0.2. (a). The grid voltages. (b). Capacitor voltages od phase C. (c). Three-phase output currents. (d). output voltage references.

Two experimental cases are included, where the swell depth of the grid voltages are 0.2 and 0.4 individually.

The experimental results of Case 1 are shown in Fig. 11, and the amplitude output currents are set at 1 A. As is shown in Fig. 11 (a), before 0.9 s, the amplitudes of the grid voltages are about 30 V. At the time of about 0.9 s, the grid voltage swell occurs and the amplitude of the grid voltage in phase C
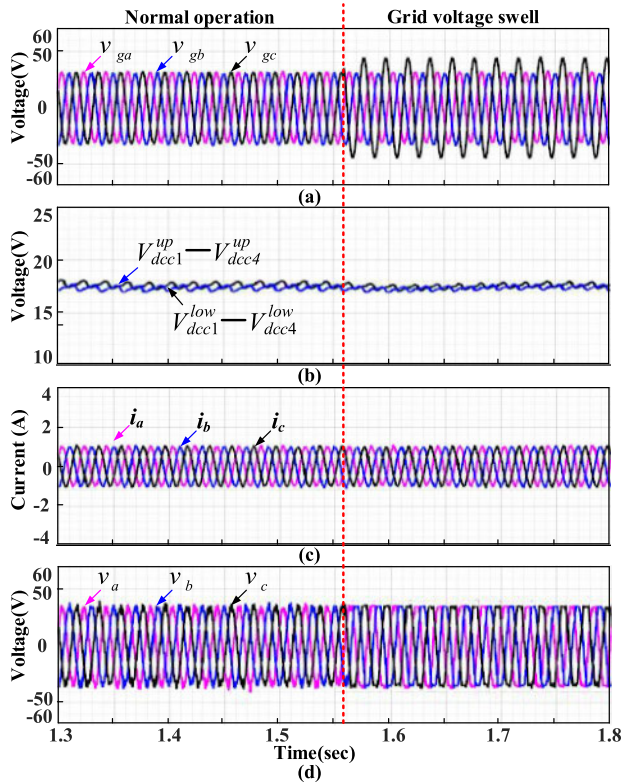
FIGURE 12. Experimental waveforms of proposed operation approach under grid voltage swell with depth of 0.4. (a). The grid voltages. (b). Capacitor voltages od phase C. (c). Three-phase output currents. (d). output voltage references.

rises to 36 V. The capacitor voltages are shown in Fig. 11 (b), where the capacitor voltage stabilizes at about 17.5 V before and after the grid voltage swell, indicating the effectiveness of the proposed operation approach in regulating capacitor voltages. Fig. 11 (c) shows the output currents. It can be seen from the figure that before and after the grid voltage swell, the amplitudes of the output currents are both 1 A, and there is almost no current distortion after grid voltage swell. It verifies that the proposed operation approach can precisely track the output current references even under grid voltage swell. Fig. 11 (d) shows the three-phase output references. It can be seen that before 0.9 s, the amplitudes of the output references are almost the same with that of the grid voltages. After 0.9 s, the amplitude of the output voltage reference in the faulty phase is much lower than the amplitude of that of the phase-to-ground voltage, due to the injection of ZSV. The effectiveness of the proposed operation approach is thus verified with $D = 0.2$ for a grid voltage swell.

The experimental results of Case 2 are shown in Fig. 12, and the amplitude of the output currents are set the same as 1 A. As is shown in Fig. 12 (a), before 1.56 s, the amplitudes of the grid voltages are about 30 V. At the time of about 1.56 s, the grid voltage swell occurs and the amplitude of the grid voltage in phase C rise to 42 V. Fig. 12 (b) shows the capacitor voltages, where the capacitor voltage remain stable at about 17.5 V during both normal operation and grid swell occasion, validating the effectiveness of the

proposed operation approach in regulating capacitor voltages. Fig. 12 (c) gives the output currents. It can be seen from the figure that before and after the grid voltage swell, the amplitudes of the output currents are both 1 A, and there is almost no current distortion after the grid voltage swell, indicating the proposed operation approach can effectively control the output current references even under grid voltage swell. Fig. 12 (d) shows the three-phase output references, where it can be seen that before 1.56 s, the amplitudes of the output references are almost the same with that of the grid voltages. After 1.56 s, the amplitude of the output voltage reference in the faulty phase is much lower than the amplitude of that in the phase-to-ground voltage, and is clamped to the maximum output value, due to the injection of FZSV and IZSV. The experimental results demonstrate the effectiveness of the proposed operation approach with $D = 0.4$ for a grid voltage swell.

VI. CONCLUSION
By the combination of fundamental and irregular zero-sequence voltage injection, this paper proposes a simple operation approach to keep MMC normal operation under grid voltage swell. The contribution of the proposed method includes:

1. The fundamental ZSV injection can guarantee the same amplitude of the modulation waves of three phases, and keep the same modulation margin;

2. With the irregular ZSV injection, the tolerance ability of MMC is further improved under severe grid voltage swell.

3. High-quality waveforms of the line-to-line voltages and output currents can be guaranteed.

Simulation and experimental results show that the proposed scheme can realize fault ride-through operation of MMC under different grid-voltage swell conditions.

REFERENCES
[1] Y. Wang, Q. Song, B. Zhao, J. G. Li, Q. H. Sun, and W. H. Liu, "Quasi-square-wave modulation of modular multilevel high-frequency DC converter for medium-voltage DC distribution application," *IEEE Trans. Power Electron.*, vol. 33, no. 9, pp. 7480–7495, Sep. 2018.

[2] L. Chen, S. Shao, Q. Xiao, L. Tarisciotti, T. Dragicevic, and P. Wheeler, "Model-predictive-control for dual-active-bridge converters supplying pulsed power loads in naval DC microgrids," *IEEE Trans. Power Electron.*, to be published.

[3] Q. Xiao, L. Chen, H. Jia, P. Wheeler, and T. Dragicevic, "Model predictive control for dual-active-bridge in naval DC micro-grids supplying pulsed power loads featuring fast transition and online transformer current minimization," *IEEE Trans. Ind. Electron.*, to be published.

[4] J. Lamb, B. Mirafzal, and F. Blaabjerg, "PWM common mode reference generation for maximizing the linear modulation region of CHB converters in islanded microgrids," *IEEE Trans. Ind. Electron.*, vol. 65, no. 7, pp. 5250–5259, Jul. 2018.

[5] H. Jia, Q. Xiao, and J. He, "An improved grid current and DC capacitor voltage balancing method for three-terminal hybrid AC/DC microgrid," *IEEE Trans. Smart Grid*, to be published.

[6] J. Rocabert, A. Luna, F. Blaabjerg, and P. Rodriguez, "Control of power converters in AC microgrids," *IEEE Trans. Power Electron.*, vol. 27, no. 11, pp. 4734–4749, Nov. 2012.

[7] J. Fang, Y. Tang, H. Li, and X. Li, "A battery/ultracapacitor hybrid energy storage system for implementing the power management of virtual synchronous generators," *IEEE Trans. Power Electron.*, vol. 33, no. 4, pp. 2820–2824, Apr. 2018.

[8] J. Wang, J. Liang, C. Wang, and X. Dong, "Circulating current suppression for MMC-HVDC under unbalanced grid conditions," *IEEE Trans. Ind. Appl.*, vol. 53, no. 4, pp. 3250–3259, Jul./Aug. 2017.

[9] Y. Jin, Q. Xiao, C. Dong, H. Jia, Y. Mu, B. Xie, Y. Ji, S. K. Chaudhary, and R. Teodorescu, "A novel submodule voltage balancing scheme for modular multilevel cascade converter—Double-star chopper-cells (MMCC-DSCC) based STATCOM," *IEEE Access*, vol. 7, pp. 83058–83073, Jun. 2019.

[10] S. Du, B. Wu, and N. R. Zargari, "A star-channel modular multilevel converter for zero/low-fundamental-frequency operation without injecting common-mode voltage," *IEEE Trans. Power Electron.*, vol. 33, no. 4, pp. 2857–2865, Apr. 2018.

[11] Y. Chen, S. Zhao, Z. Li, X. Wei, and Y. Kang, "Modeling and control of the isolated DC–DC modular multilevel converter for electric ship medium voltage direct current power system," *IEEE J. Emerg. Sel. Topics Power Electron.*, vol. 5, no. 1, pp. 124–139, Mar. 2017.

[12] N. Li, F. Gao, T. Hao, Z. Ma, and C. Zhang, "SOH balancing control method for the MMC battery energy storage system," *IEEE Trans. Ind. Electron.*, vol. 65, no. 8, pp. 6581–6591, Aug. 2018.

[13] B. Fan, Y. Li, K. Wang, Z. Zheng, and L. Xu, "Hierarchical system design and control of an MMC-based power-electronic transformer," *IEEE Trans. Ind. Informat.*, vol. 13, no. 1, pp. 238–247, Feb. 2017.

[14] S. Yang, J. Fang, Y. Tang, H. Qiu, C. Dong, and P. Wang, "Modular multilevel converter synthetic inertia-based frequency support for medium-voltage microgrids," *IEEE Trans. Ind. Electron.*, vol. 66, no. 11, pp. 8992–9002, Nov. 2019.

[15] Z. Xie, X. Zhang, X. Zhang, S. Yang, and L. Wang, "Improved ride-through control of DFIG during grid voltage swell," *IEEE Trans. Ind. Electron.*, vol. 62, no. 6, pp. 3584–3594, Jun. 2015.

[16] D. Campos-Gaona, E. L. Moreno-Goytia, and O. Anaya-Lara, "Fault ride-through improvement of DFIG-WT by integrating a two-degrees-of-freedom internal model control," *IEEE Trans. Ind. Electron.*, vol. 60, no. 3, pp. 1133–1145, Mar. 2013.

[17] F. K. A. Lima, A. Luna, P. Rodriguez, E. H. Watanabe, and F. Blaabjerg, "Rotor voltage dynamics in the doubly fed induction generator during grid faults," *IEEE Trans. Power Electron.*, vol. 25, no. 1, pp. 118–130, Jan. 2010.

[18] X. Guo, W. Liu, X. Zhang, X. Sun, Z. Lu, and J. M. Guerrero, "Flexible control strategy for grid-connected inverter under unbalanced grid faults without PLL," *IEEE Trans. Power Electron.*, vol. 30, no. 4, pp. 1773–1778, Apr. 2015.

[19] (Oct. 21, 2008). *Australian Energy Market Commission, National Electricity Rules[R/OL]*. [Online]. Available: http://www.aemc. gov.au

[20] M. N. Eskander and S. I. Amer, "Mitigation of voltage dips and swells in grid-connected wind energy conversion systems," in *Proc. ICCAS-SICE*, Fukuoka, Japan, Aug. 2009, pp. 885–890.

[21] C. Wessels and F. W. Fuchs, "High voltage ride through with FACTS for DFIG based wind turbines," in *Proc. IEEE EPE*, Barcelona, Spain, Sep. 2009, pp. 1–10.

[22] C. Feltes, S. Engelhardt, J. Kretschmann, J. Fortmann, F. Koch, and I. Erlich, "High voltage ride-through of DFIG-based wind turbines," in *Proc. IEEE PES-GM*, Pittsburgh, PA, USA, Jul. 2008, pp. 1–8.

[23] J. Yang, J. E. Fletcher, and J. O'Reilly, "A series-dynamic-resistor-based converter protection scheme for doubly-fed induction generator during various fault conditions," *IEEE Trans. Energy Convers.*, vol. 25, no. 2, pp. 422–432, Jun. 2010.

[24] M. Mohseni and S. M. Islam, "Transient control of DFIG-based wind power plants in compliance with the australian grid code," *IEEE Trans. Power Electron.*, vol. 27, no. 6, pp. 2813–2824, Jun. 2012.

[25] R. P. Burgos and E. P. Wiechmann, "Extended voltage swell ride-through capability for PWM voltage-source rectifiers," *IEEE Trans. Ind. Electron.*, vol. 52, no. 4, pp. 1086–1098, Aug. 2005.

[26] B. Li, Z. Xu, J. Ding, and D. Xu, "Fault-tolerant control of medium-voltage modular multilevel converters with minimum performance degradation under submodule failures," *IEEE Access*, vol. 6, pp. 11772–11781, 2018.

[27] K. Sharifabadi, L. Harnefors, H.-P. Nee, S. Norrga, and R. Teodorescu, *Design, Control, and Application of Modular Multilevel Converters for HVDC Transmission Systems*, 1st ed. Hoboken, NJ, USA: Wiley, 2016.

[28] M. Hagiwara and H. Akagi, "Control and experiment of pulsewidth-modulated modular multilevel converters," *IEEE Trans. Power Electron.*, vol. 24, no. 7, pp. 1737–1746, Jul. 2009.

[29] M. R. Alam, K. M. Muttaqi, and A. Bouzerdoum, "Characterizing voltage sags and swells using three-phase voltage ellipse parameters," *IEEE Trans. Ind. Appl.*, vol. 51, no. 4, pp. 2780–2790, Jul./Aug. 2015.
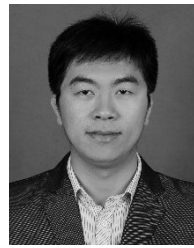
QIAN XIAO received the B.S. and M.S. degrees in electrical engineering from the Hebei University of Technology, Tianjin, China, in 2011 and 2014, respectively. He is currently pursuing the Ph.D. degree in electrical engineering, Tianjin University, Tianjin.

Since November 2018, he has been a Visiting Researcher with the Department of Energy Technology, Aalborg University, Aalborg, Denmark. His research interests are multilevel converters, DC/DC converters, and power electronics for distributed generation, microgrid, and HVDC.

YU JIN was born in Heilongjiang, China, in 1994. He received the B.S. degree from the School of Electrical Engineering and Automation, Harbin Institute of Technology, Harbin, China, in 2015. He is currently pursuing the Ph.D. degree with the School of Electrical Engineering and Automation, Harbin Institute of Technology.

Since October 2018, he has been a Visiting Researcher with the Department of Energy Technology, Aalborg University, Aalborg, Denmark. His current research interests include modular multilevel converters and the applications in microgrid.

LINGLIN CHEN received the M.Sc. degree in electrical engineering from Zhejiang University, Hangzhou, China, in 2016. He is currently pursuing the Ph.D. degree with the Power Electronics, Machine and Control (PEMC) Group, University of Nottingham, U.K.

He was a Visiting Scholar with the Department of Energy Technology, Aalborg University, Aalborg, Denmark. His current research interests include high power AC/DC converters, high current DC/DC power converters, model predictive control, and power system in more electric aircrafts.

XIAODAN YU was born in Liaoning, China. She received the B.S., M.S., and Ph.D. degrees in the electrical engineering from Tianjin University, Tianjin, China, in 1996, 1998, and 2013, respectively, where she is currently an Associate Professor. Her research interests include power system stability analysis, nonlinear dynamic circuit, and the optimal operation of power system.

HONGJIE JIA received the Ph.D. degree in electrical engineering from Tianjin University, China, in 2001.

He became an Associate Professor at Tianjin University, in 2002, and was promoted as a Professor, in 2006. His research interests include power reliability assessment, stability analysis and control, distribution network planning and automation, and smart grids.

HUIQIAO LIU received the B.S. and M.S. degrees in electrical engineering from the Hebei University of Technology, Tianjin, China, in 2011 and 2014, respectively.

She became a Teacher at Zhonghuan Information College, Tianjin University of Technology, Tianjin, in 2014. Her research interests include multilevel converters and microgrid.

REMUS TEODORESCU (S'94–M'99–SM'02–F'12) received the Dipl.Ing. degree in electrical engineering from the Polytechnical University of Bucharest, Romania, in 1989, and the Ph.D. degree in power electronics from the University of Galati, Romania, in 1994.

In 1998, he joined Power Electronics Section, Department of Energy Technology, Aalborg University, where he is currently a Professor. From 2013 to 2017, he was a Visiting Professor with Chalmers University. He was the Coordinator of Vestas Power Program from 2007 to 2013, involving ten Ph.D. projects in the areas of power electronics, power systems, and energy storage. He has co-authored the book *Grid Converters for Photovoltaic and Wind Power Systems*, (Wiley, 2010) and more than 400 IEEE journals and conference articles. His areas of interests include design and control of power converters for photovoltaics and wind power systems, grid integration with wind power, HVDC/FACTS based on MMC, SiC-based converters, and storage systems for utility.

FREDE BLAABJERG (S'86–M'88–SM'97–F'03) received the Ph.D. degree in electrical engineering from Aalborg University, in 1995. He is currently pursuing the honoris causa degree with University Politehnica Timisoara (UPT), Romania, and Tallinn Technical University (TTU), Estonia.

He was with ABB-Scandia, Randers, Denmark, from 1987 to 1988. He became an Assistant Professor, in 1992, an Associate Professor, in 1996, and a Full Professor of power electronics and drives, in 1998. In 2017, he became a Villum Investigator. He has published more than 600 journal articles in the fields of power electronics and its applications. He is the coauthor of four monographs and editor of ten books in power electronics and its applications. His current research interests include power electronics and its applications, such as in wind turbines, PV systems, reliability, harmonics, and adjustable speed drives.

He has received 30 IEEE Prize Paper Awards, the IEEE PELS Distinguished Service Award, in 2009, the EPE-PEMC Council Award, in 2010, the IEEE William E. Newell Power Electronics Award, in 2014, the Villum Kann Rasmussen Research Award, in 2014, and the Global Energy Prize, in 2019. He was the Editor-in-Chief of the IEEE Transactions on Power Electronics, from 2006 to 2012. He has been Distinguished Lecturer for the IEEE Power Electronics Society, from 2005 to 2007, and for the IEEE Industry Applications Society, from 2010 to 2011 and 2017 to 2018. Since 2019, he has been the President of IEEE Power Electronics Society. He is the Vice-President of the Danish Academy of Technical Sciences too. He was nominated by Thomson Reuters to be between the most 250 cited researchers in Engineering in the world, from 2014 to 2018.

• • •